Multilayer perceptron neural network and eddy current technique for estimation of the crack depth on massive metal structures

Bui Tien Dat, Pham Van Dung, Cung Thanh Long*

Hanoi University of Science and Technology.
*Corresponding author: long.cungthanh@hust.edu.vn.
Received 08 November 2021; Revised 27 January 2022; Accepted 14 February 2022.
DOI: https://doi.org/10.54939/1859-1043.j.mst.77.2022.3-12

ABSTRACT

This paper introduces a method for estimating the maximum depth (sub-millimeter) of minor cracks on the surface of aluminum plates used in the aeronautical industry. A set of C-scan eddy current (EC) images, including real and imaginary parts of the impedance, is analyzed to extract suitable features after reducing noise effects, such as background noises and edge noises. Based on the obtained features, e.g. maximum impedance, the background feature, background noises, type of sensors, a Multilayer Perceptron (MLP) Neural Network is built to estimate the maximum depth of the cracks. The network is optimized based on loss functions, such as mean absolute error and mean squared error. An optimal network structure with five neurons in the first hidden layer and eight neurons in the second hidden layer is chosen. The obtained result indicated that the relative error of estimations is lower than 10% for almost all experimental tested samples.

Keywords: Non-destructive evaluation; Eddy-current technique; Feature extraction; Multi-frequency approach; Multilayer perceptron (MLP) neural network.

1. INTRODUCTION

In aeronautical industry and services, the fuselage structures that use a laminated metal structure are often at risk of damage due to the emergence of minor cracks under the influence of complex working conditions. Therefore, early detection of cracks appearing in the aircraft's fuselage has a significant role in aviation safety. In many other industrial sectors, the problem of detecting and quantifying damages in metal parts is also of great importance in manufacturing, as well as in the operation and maintenance of equipment. Non-Destructive Testing/ Estimation (NDT/E) method using eddy current is one of the most widely applied methods for this task[1].

The advantage of the eddy current NDT/E is high sensitivity and mobility. It has the ability to detect defects on and below the object's surface. Moreover, it does not require a complex preparation on tested surfaces [2, 3]. Therefore, the NDT/E method using eddy current is widely applied to determine qualitatively as well as quantitatively defects on metal structures, such as evaluation of surface corrosion of gas pipelines [4-7], inspection of structures in aerospace industry [8-10], maintenance of steel plates in road and bridge construction [11-13] or steel-pipes used in many different fields [14, 15].

Many attempts have been made to identify cracks in various massive metal structures. Here are some published results for this research field. Ehsan Mohseni [16] improved the reliability of the ECT by using a split-D reflection differential probe. This solution allows for good working with noises such as surface roughness and frequency of measurements. Marko Jesenik and Mladen Trlep proposed an approach [17] for determining the length and depth of cracks in conductive metal plates. In their approach, the position of the crack is detected through the relationship between the changes in the magnetic density of the measuring points, and the depth is determined using the FEM model. Meanwhile, a method is proposed by Zhenwei Wang and Yating Yu [18] that uses both traditional eddy current (TEC) (harmonic excitation) and pulse eddy current (PEC) simultaneously to estimate multiple crack chains in metal specimens

(Multiple Micro - Cracks). In this approach, the TEC technique is used to locate the cracks, while the PEC is used to estimate the depth.

Machine learning techniques are also applied to improve the quality of inspection and evaluation of cracks in metal parts. Lulu Titan [19] introduced a statistical approach to extract the best data in the eddy current dataset measured under the influence of noise. The author used Principal Component Analysis (PCA) method to select features. Faris Nafiah and Ali Sophian published a method of crack angular detection, based on the processing of 2D images, and using the convolutional neural network (CNN) [20]. In their approach, three features LLS (length of extracted linear scans), LSS (linear scan skewness), and LSmax (highest value on linear scan) are extracted from scanned images. They are used to determine the depth and rib inclination of cracks. Another work was implemented by Milan Smetana [21]. The author combined wavelet transform and MLP network to estimate crack depth. For obtained results, the error is less than 10%, under noisy conditions with the SNR up to 10 dB.

The size of cracks in most of the above publications is several millimeters. Very few studies have been done with crack depth smaller than 1 mm. In our previous work [22], we propose an approach using a polynomial model to estimate crack depth in the range from 200 to 800 µm, through the processing of S-scan EC signals. The mean error over the entire range is about 10%.

With the same problem in [22], in this paper, we use MLP network when working with larger and less centralized datasets. The used data are the scans of the object's surface, using absolute and differential eddy current sensors, operating at two frequencies of 400 kHz and 500 kHz. The standard crack depth ranges from 200 µm to 800 µm. From the obtained experimental images, we implement a pre processing procedure to reduce the effects of background noise and edge noise before extracting features of signals. To estimate the maximum crack depth, a MLP neural network is used, with the input being a vector of features extracted from the image processing steps.

The following sections of this paper are organized as follows: Section 2 presents techniques to reduce the effect of noise on measurement data and feature extraction. Section 3 describes the structure and hyperparameters of the MLP network obtained from optimization results. Section 4 presents and evaluates the estimated results. Finally, section 5 are some conclusions and our future works.

2. PREPROCESSING AND FEATURE EXTRACTION

2.1. Problem formulation

The data are stored as matrices of the real and imaginary parts of the impedance on the measuring surface. As an example, figure 1 shows an image of the real part of sensor impedance. In this case, an absolute sensor was scanned on a tested surface to obtain data corresponding to a standard crack depth of about 800 µm, due to the affection of the third fatigue period.

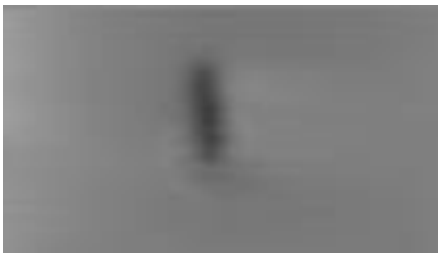

Figure 1. *Image of the real part of the impedance of an absolute sensor measured on a sample with a crack depth of 800 µm.*

Data were compiled from measurements on eight test samples. The test pieces are divided into two groups (denoted A and B) corresponding to 2 types of mechanical force acting on

samples. Each group consists of 4 samples and is numbered from 1 to 4. For example, the second pattern of the first group is called model A2. Each test piece is subjected to three fatigue cycles to produce three standard maximum depths of 200, 400, and 800 µm, correspondingly.

After each cycle of mechanical stimulation, the specimen surface is scanned by using eddy current sensors to collect data. The results are C-scans images, in TIF format, showing the impedance value of the sensor, through files of their real parts and imaginary parts.

The data pre processing procedure includes the computation of the impedance module, the removal of background noise and edge noise, the normalization of background and area of tested surface, before extracting suitable features.

2.2. Noise treatment and normalization

The dataset contains noise which is the change of impedance around the crack. Some of the reasons are that the tested surface is affected by an external force during crack formation; the sensor is influenced by undetermined factors when performing measurements. Figure 2 shows the effect of noise on the test sample A2, in which figure 2a shows the real part, and 2b shows the imaginary part of the sensor impedance. For this measurement, an absolute sensor operating at the frequency of 500 kHz is used.

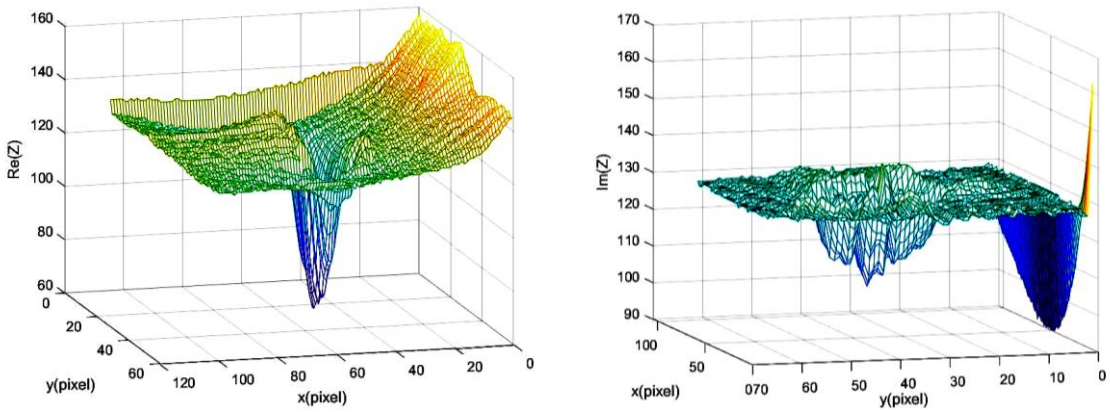

(a) (b)

Figure 2. *Image of the real (a) and imaginary (b) parts of the impedance of the absolute sensor operating on the sample A2 with a depth of 800 µm.*

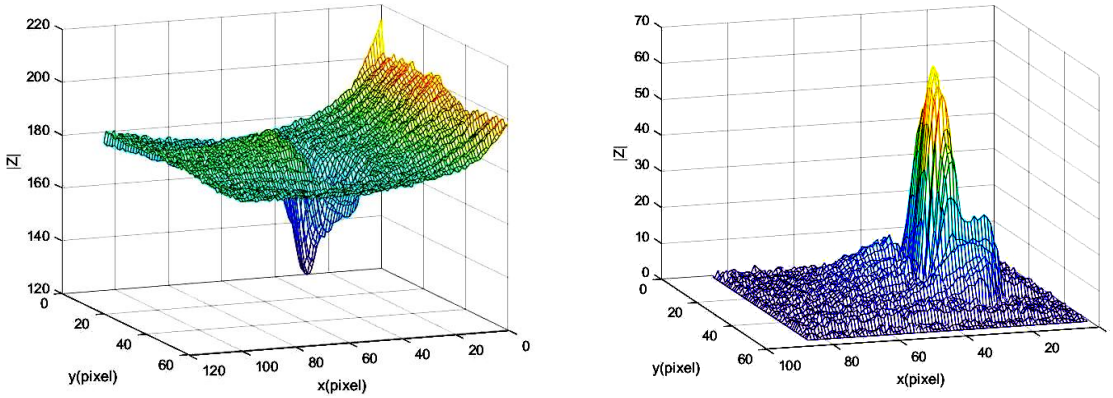

a) b)

Figure 3. *Impedance module before a) and after noise removal and background normalization b).*

Edge noise on each sample appears at the surface boundary due to the change in the moving

direction of the sensor, the difference between impedance of the tested surface and the surrounding environment, etc., leading to an abnormal change in values of sensor impedance. However, this effect exists on a small area close to the image edges and is easily eliminated by simple cropping. As an example, the impact of edge noise on the result of a test is in figure 3.

The objective of surface noise treatment is to reduce the effect of background noises and edge noises. Due to the difference in the size of impedance images, the edge noise treatment also standardizes the area of all images. After removing the edge noise, the images have the same size of (19, 61) pixels (figure 4). The average value of the sensor impedance outside the area which is affected by mechanical force calls the background impedance. We normalize the image background by suppressing the background impedance of each image.

By this way, the background of all images is normalized to zero. On the normalized data, the relationship between crack depth and the impedance value, at the position where the crack appears, will be investigated. Figure 5 shows the normalized data, taken on sample A2 at the third fatigue cycle, using a differential sensor.

Numbers of features will be extracted from the normalized data. They are used as inputs for MLP networks to estimate the maximum crack depth.

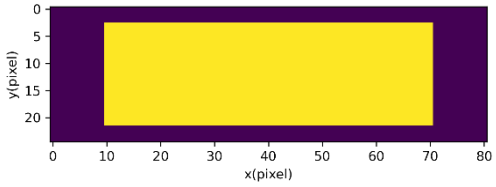

Figure 4. *Image size normalization: outer (darkened) outlines are removed.*

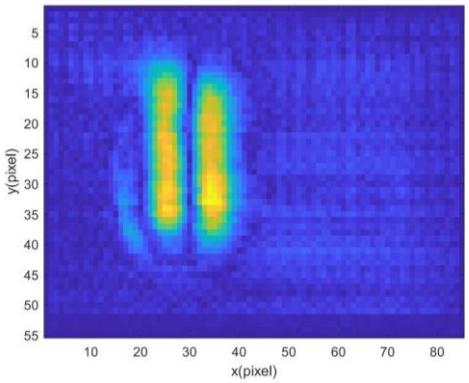

Figure 5. *An impedance image after noise removal and background normalization (sample A2, third fatigue cycle, using the differential sensor to collect data).*

2.3. Feature extraction

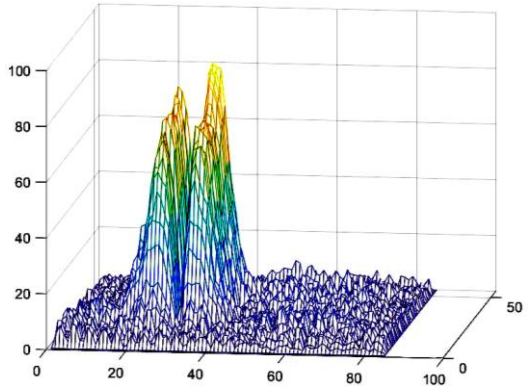

Figure 6. *The impedance matrix of a differential sensor has two peaks with different maximum values.*

The feature of maximum impedance (Z_{max}) is the maximum element (impedance module) of

the normalized impedance matrix, as shown in equation (1). For the impedance matrix of a differential sensor, there are two peaks, and Z_{max} is chosen as the larger one (figure 6).

$$Z_{max} = \max(\hat{Z}_{i,j}) \tag{1}$$

where $\hat{Z}_{i,j}$ is the element at the i^{th} row and the j^{th} column of the impedance module matrix after normalization.

The background feature (Z_{ground}) provides information on the surface of a tested sample and is calculated as equation (2). The positions with the non-zero background may correspond to a lift-off between the tested surface and the sensor [18]. Note that if the value of impedance at non-crack locations is large, it will affect to Z_{max} feature. Assuming we have two tested samples. The first specimen has a crack of 800 µm deep, and the second one has a crack of 200 µm deep, respectively. They have the same value of Z_{max} (equal to 20, for example). However, the sample with a crack depth of 800 µm has $Z_{ground} = 7$, meanwhile, the one with a crack depth of 200 µm has $Z_{ground} = 1.2$. It indicates that the value Z_{max} of the first sample is affected by the procedure of background suppression. The large value Z_{ground} may be caused by the large dropped surface around the crack or caused by the larger opened section, the longer and sharper slope of the 800 µm crack compared to that of 200 µm crack. The feature Z_{ground} also shows the formation characteristic of cracks under different mechanical impacts.

$$Z_{ground} = \frac{1}{l \times g}\left(\sum_{i=1}^{l}\sum_{j=1}^{g}\hat{Z}_{i,j}\right) \tag{2}$$

where l is the number of rows of the impedance matrix, and g is equal to one third of the number of columns of the impedance matrix.

The feature Z_{noise} (background noise) represents the variation range of background impedances around the mean value. This feature is the standard deviation of background impedance values, calculated as in equation (3). Some tested samples have large Z_{ground} but small Z_{noise}, and vice versa. The measurement data shows a clear difference of this feature on each tested sample, with cracks having different depths. In other words, this feature gives information about both the surface of tested samples and the depth of cracks.

$$Z_{noise} = \frac{1}{l}\sum_{i=0}^{l} s_{(i,1,n)} \tag{3}$$

where

$$s_{(x,y,z)} = \sqrt{\frac{\sum_{j=y}^{y+z}(\hat{Z}_{x,j} - \frac{1}{z}(\sum_{j=y}^{y+z}\hat{Z}_{x,j}))^2}{z-1}} \tag{4}$$

is the standard deviation of the impedance values $\hat{Z}_{x,j}$ in the x^{th} row from the y^{th} to $(y+z)^{th}$ column.

The maximum crack depth can be related not only to the Z_{max} value, but also to the mean value of sensor impedances around the position of Z_{max} (called Z_{mean}) and the variation speed of the impedance around that position (called Z_{slope}). These features provide information about the shape and the size of cracks.

The feature Z_{mean}, calculated as in equation (5), is the mean value of five elements next to the element Z_{max} in an impedance matrix. This value (compared to Z_{max}) can provide information about the shape of the crack around its deepest point.

$$Z_{mean} = \frac{1}{(2p+1)^2}\left(\sum_{i=ml-p}^{i=ml+p}\sum_{j=mc-p}^{j=mc+p}\hat{Z}_{i,j}\right) \quad (5)$$

where (ml, mc) is the position coordinate of the maximum impedance value and p is the number of pixels adjacent to the element Z_{max} (in this paper, we set $p = 2$).

The feature Z_{slope} is calculated as in equation (6), which is the mean value of standard deviation on five impedance rows, around the position of Z_{max}. In which, the value in each row is the standard deviation of five elements around Z_{max}. Z_{slope} represents the narrow of the crack bottom. The larger this value the steeper the crack, and vice versa.

$$Z_{slope} = \frac{1}{2p+1}\sum_{i=ml-p}^{ml+p} s_{(i,mc,p)} \quad (6)$$

In this paper, we use an additional (digital) characteristic to distinguish the type of sensors. Specifically, 0 corresponds to the sensor working at the frequency of 400 kHz, and 1 for the one working at the 500 kHz.

3. NETWORK CONSTRUCTION AND TRAINING

We use the traditional MLP network (figure 7) for this application, because the number of samples for training is small. At the same time, the MLP network is considered universal, used well for complex classification problems. Since the output values are between 0 and 1, the activation function for the first hidden layer is chosen as the sigmoid function. On the other hand, since the features of cracks and the output value are positive, the activation function for the remaining hidden layers will be chosen as a tang-hyperbolic function (tanh), because this function is always non-negative.

The dataset is divided into two parts: the training set and the test set. The test set includes samples with three different crack depths (200 µm, 400 µm, and 800 µm), measured with both types of sensors (absolute and differential type), operating at two different frequencies (400 kHz and 500 kHz). Due to the limitation of data, this set consists of six elements. Meanwhile, the training set includes 42 different learning patterns.

The optimization of network configuration is performed by fixing the activation function of neurons, changing the number of hidden layers, the number of neurons in each hidden layer, and evaluating the learning speed of network. Network parameters are optimized by using Mean Square Error (MSE) function (equation 7) and ADAM method.

$$MSE = \frac{1}{n}\sum_{i=1}^{n}(p - \hat{p})^2 \quad (7)$$

where $\hat{p}$ and p are the estimation results and actual values of the crack depth.

Grid Search method [24], K-Fold algorithm (with 8 folds) are used to train and validate the networks. To stop training before overfitting occurs, the Early Stopping method is used [20].

We tested 3 network configurations with the number of hidden layers are 2, 3, and 4, respectively. Results from figure 8 show that the network with 2 hidden layers has the smallest MSE, and the smallest difference of error on each tested sample. With three hidden layer

network, the MSE is as low as that of the two hidden layer network, but the error on some samples is greater than 10%. The model with four hidden layers gives the largest errors due to overfitting. The overfitting occurs on this model, because the configuration of network is too large to the training data set. Thereby, we choose to use the network with two hidden layers.

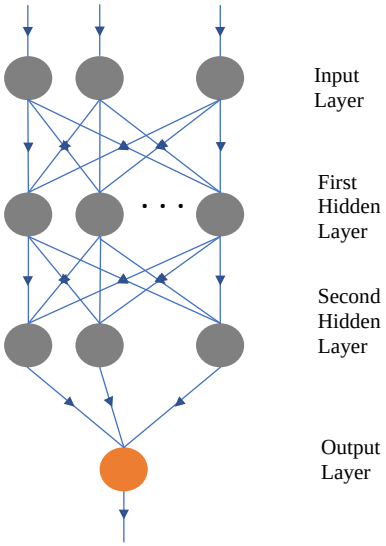

Figure 7. *One type of MLP network structure.*

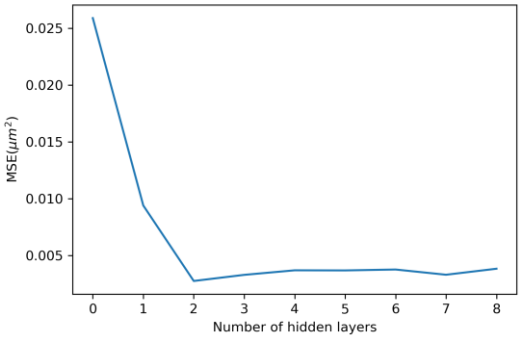

Figure 8. *Optimizing the number of hidden layers.*

For the chosen configuration of the network, using the default learning rate $(1e-3)$, we optimize the number of neurons in each hidden layer. The number of neurons is tested from 1 to 15. Table 1 shows three tested configurations (6:5:5:1; 6:5:8:1; 6:5:15:1) and their ability, evaluated through the Mean Absolute Relative Error (MARE), and the Root Mean Square Error (RMSE) as indicated in Equation 8 and Equation 9, respectively.

$$MARE = \frac{1}{n}\sum_{i=1}^{n}\left|\frac{p-\hat{p}}{p}\right|.100 \tag{8}$$

$$RMSE = \sqrt{\frac{1}{n}\sum_{i=1}^{n}(\hat{p}-p)^2} \tag{9}$$

where $\hat{p}$ and p are the estimation results and actual values of the crack depth.

Table 1. *Optimizing the number of hidden layers and the number of neurons in each hidden layer.*

MLP ANN	MARE (%)	RMSE (μm)
6:5:5:1	8.57	49.94
6:5:8:1	4.87 ($MARE_{min}$)	37.13 ($RMSE_{min}$)
6:5:15:1	5.29	39.75
6:5:5:5:1	11.39	70.99
6:5:5:10:1	13.27	79.82
6:5:5:15:1	15.48	91.52

In this way, we obtain an optimal network structure with five neurons in the first hidden layer and eight neurons in the second hidden layer.

4. RESULTS AND DISCUSSION

To evaluate estimation results, we use three quantities: root mean squared error (RMSE), mean relative error (MRE), and mean precision error (MPE). The RMSE provides overall information on the accuracy of the estimation method at all different measurement points. However, this quantity does not directly reflect the relative error (RE) of estimation results at different depths. So, we use two other quantities MRE and MPE, defined as in equation (10) and (11), to characterize the estimation method.

$$MRE\% = mean(\frac{\hat{p} - p}{p}.100) \tag{10}$$

where $\hat{p}$ and p are the estimation results and actual values of the crack depth.

$$MPE = \sqrt{\frac{\sum_{i=1}^{n}(RE_i - MRE)^2}{n}} \tag{11}$$

Note that, the value of RE and therefore MRE can be negative or positive, indicating that the estimated values may be smaller or larger than the actual values. The MPE shows the variation of RE around the mean value of RE.

The estimation results on 6 tested samples, for 3 standard depth of cracks (200, 400 and 800 µm), and using the optimal network are good enough, as shown in table 2.

Tested results show that the RE is in the range of 0.6% to 8.57%. The mean variation of REs is only 3.19%. RMSE on all three different depths (200, 400 and 800 µm) is 32.14 µm. These results indicate the high reliability, high accuracy of individual estimations, and the proposed estimation method.

The experiments also showed that the greater the depth of the crack, the more accurate the estimation results. For the depth of 200 µm, the mean relative error is about 7%, while that kind of error for the crack depth of 800 µm is only 2%. In other words, the greater the depth of the crack, the easier to estimate accurately. The tested results show that our proposed approach is good enough even for cracks with small depth, and therefore, having a good potential to apply to industrial practices.

Table 2. *Some test results of estimation method.*

MRE (%)	4.47
Max RE (%)	8.57
Min RE (%)	0.60
MPE (%)	3.19
RMSE (µm)	32.14

5. CONCLUSION

This paper presented a method to estimate the depth of sub-millimeter cracks on the surface of a massive metal structure. The good estimation results show that the noise treatment and the feature extraction as proposed in the paper are appropriate. All maximum relative errors do not exceed 10%, for all tested samples, at all different depth of cracks (200, 400, and 800 µm).

In following studies, we consider the relationship between maximum depth with opened surface area, slope of wall crack, and volume of crack, to extract more features that allow quantification of other geometric parameters of cracks. In addition, the reconstruction of 3D images of cracks is also considered.

REFERENCES

[1]. N. Yusa, H. Huang, and K. Miya, "*Numerical evaluation of the ill-posedness of eddy current problems to size real cracks,*" NDT & E International, **Vol. 40**, no. 3, pp. 185–191, (2007).

[2]. M. Zergoug, S. Lebailia, and G. Kamel, "*Characterization of the corrosion by eddy current,*" p. 7.

[3]. D. C. Copley, "*Eddy-Current Imaging for Defect Characterization,*" in Review of Progress in Quantitative Nondestructive Evaluation, D. O. Thompson and D. E. Chimenti, Eds. Boston, MA: Springer US, pp. 1527–1540 (1983).

[4]. L. Xie, B. Gao, G. Y. Tian, J. Tan, B. Feng, and Y. Yin, "*Coupling pulse eddy current sensor for deeper defects NDT,*" Sensors and Actuators A: Physical, **Vol. 293**, pp. 189–199, (2019).

[5]. D. Kim, L. Udpa, and S. Udpa, "*Remote field eddy current testing for detection of stress corrosion cracks in gas transmission pipelines,*" Materials Letters, **Vol. 58**, no. 15, pp. 2102–2104, (2004).

[6]. S. Xie, Z. Duan, J. Li, Z. Tong, M. Tian, and Z. Chen, "*A novel magnetic force transmission eddy current array probe and its application for nondestructive testing of defects in pipeline structures,*" Sensors and Actuators A: Physical, **Vol. 309**, p. 112030, (2020).

[7]. Z. Chu, Z. Jiang, Z. Mao, Y. Shen, J. Gao, and S. Dong, "*Low-power eddy current detection with 1-1 type magnetoelectric sensor for pipeline cracks monitoring,*" Sensors and Actuators A: Physical, **Vol. 318**, p. 112496, (2021).

[8]. Y. He *et al.*, "*Pulsed eddy current technique for defect detection in aircraft riveted structures,*" NDT & E International, **Vol. 43**, no. 2, pp. 176–181, (2010).

[9]. J. H. Espina-Hernández, E. Ramírez-Pacheco, F. Caleyo, J. A. Pérez-Benitez, and J. M. Hallen, "*Rapid estimation of artificial near-side crack dimensions in aluminium using a GMR-based eddy current sensor,*" NDT & E International, **Vol. 51**, pp. 94–100, (2012).

[10]. Y. Le Diraison, P.-Y. Joubert, and D. Placko, "*Characterization of subsurface defects in aeronautical riveted lap-joints using multi-frequency eddy current imaging,*" NDT & E International, **Vol. 42**, no. 2, pp. 133–140, (2009).

[11]. D. J. Pasadas, A. L. Ribeiro, T. J. Rocha, and H. G. Ramos, "*Open crack depth evaluation using eddy current methods and GMR detection,*" in 2014 IEEE Metrology for Aerospace (MetroAeroSpace), pp. 117–121, (2014).

[12]. R. Menezes, A. L. Ribeiro, and H. G. Ramos, "*Evaluation of crack depth using eddy current techniques with GMR-based probes,*" in 2015 IEEE Metrology for Aerospace (MetroAeroSpace), Benevento, Italy, pp. 335–33, (2015).

[13]. K. Kwon and D. M. Frangopol, "*Bridge fatigue assessment and management using reliability-based crack growth and probability of detection models,*" Probabilistic Engineering Mechanics, **Vol. 26**, no. 3, pp. 471–480, (2011).

[14]. D. G. Park, C. S. Angani, and Y. M. Cheong, "*Differential Pulsed eddy current probe to detect the sub surface Cracks in a Stainless Steel Pipe,*" p. 6.

[15]. K. Demachi, T. Hori, and S. Perrin, "*Crack depth estimation of non-magnetic material by convolutional neural network analysis of eddy current testing signal,*" Journal of Nuclear Science and Technology, **Vol. 57**, no. 4, pp. 401–407, (2020).

[16]. E. Mohseni, D. R. França, M. Viens, W. F. Xie, and B. Xu, "*Finite Element Modelling of a Reflection Differential Split-D Eddy Current Probe Scanning Surface Notches,*" J Nondestruct Eval, **Vol. 39**, no. 2, p. 29, (2020).

[17]. M. Jesenik and M. Trlep, "*Finding a Crack and Determining Depth in a Material,*" Przegląd Elektrotechniczny, **Vol. 89**, no. 2b, pp. 64–67, (2013).

[18]. Z. Wang and Y. Yu, "*Traditional Eddy Current–Pulsed Eddy Current Fusion Diagnostic Technique for Multiple Micro-Cracks in Metals,*" Sensors (Basel), **Vol. 18**, no. 9, (2018).

[19]. L. Tian, C. Yuhua, Y. Chun, H. Xuegang, Z. Bo, and B. Libing, "*Data-Driven Method for the Measurement of Thickness/Depth Using Pulsed Eddy Current,*" Sensors and Materials, p. 1325, (2017).

[20]. F. Nafiah, A. Sophian, M. R. Khan, S. B. Abdul Hamid, and I. M. Zainal Abidin, "*Image-Based Feature Extraction Technique for Inclined Crack Quantification Using Pulsed Eddy Current,*" Chin. J. Mech. Eng., **Vol. 32**, no. 1, p. 26, (2019).
[21]. M. Smetana, L. Behun, D. Gombarska, and L. Janousek, "*New Proposal for Inverse Algorithm Enhancing Noise Robust Eddy-Current Non-Destructive Evaluation,*" Sensors (Basel), **Vol. 20**, no. 19, (2020).
[22]. L. T. Cung, T. D. Dao, P. C. Nguyen, and T. D. Bui, "*A model-based approach for estimation of the crack depth on a massive metal structure,*" Measurement and Control, **Vol. 51**, no. 5–6, pp. 182–191, (2018).
[23]. S. Jiao, J. Li, F. Du, L. Sun, and Z. Zeng, "*Characteristics of Eddy Current Distribution in Carbon Fiber Reinforced Polymer,*" Journal of Sensors, **Vol. 2016**, p. e4292134, (2016).
[24]. B. H. Shekar and G. Dagnew, "*Grid Search-Based Hyperparameter Tuning and Classification of Microarray Cancer Data,*" in 2019 Second International Conference on Advanced Computational and Communication Paradigms (ICACCP), pp. 1–8, (2019).
[25]. J. Brownlee, "*Use Early Stopping to Halt the Training of Neural Networks At the Right Time,*" Machine Learning Mastery, (2018).

TÓM TẮT

Ước lượng độ sâu vết nứt trên các cấu trúc kim loại sử dụng mạng Multilayer Perceptron và kỹ thuật dòng điện xoáy

Bài báo này trình bày một phương pháp xác định độ sâu cực đại (dưới mi-li-mét) của các vết nứt nhỏ trên bề mặt các phiến hợp kim nhôm, sử dụng trong công nghiệp hàng không. Các bức ảnh C-scan bao gồm phần ảo và phần thực của tổng trở cảm biến được phân tích nhằm trích xuất các đặc trưng phù hợp sau khi được loại bỏ các tác động bởi nhiễu, như nhiễu nền và nhiễu cạnh. Dựa vào những đặc trưng thu được như trở kháng cực đại, đặc trưng của nền, nhiễu bề mặt, loại cảm biến được sử dụng, một mạng Multilayer Perceptron (MLP) được xây dựng để ước lượng độ sâu cực đại của các vết nứt. Mô hình mạng được tối ưu hóa dựa vào các "hàm mất mát" dạng sai số tuyệt đối trung bình và sai số trung bình bình phương cực tiểu. Cấu trúc mạng tối ưu với 5 neuron ở lớp ẩn thứ nhất và 8 neuron ở lớp ẩn thứ hai được sử dụng. Kết quả thử nghiệm cho thấy sai số tương đối của các phép ước lượng nhỏ hơn 10% đối với toàn bộ dữ liệu trong tập thử nghiệm.

Từ khóa: Đánh giá không phá hủy; Trích chọn đặc trưng; Phương pháp đa tần; Mạng Perceptron nhiều lớp (MLP).